NANO LETTERS

Letter

pubs.acs.org/NanoLett

Profiling Photoinduced Carrier Generation in Semiconductor Microwire Arrays via Photoelectrochemical Metal Deposition

Mita Dasog,[†] Azhar I. Carim,[†] Sisir Yalamanchili,[‡] Harry A. Atwater,[‡] and Nathan S. Lewis*[,†,∥,⊥]

[†]Division of Chemistry and Chemical Engineering, [‡]Division of Engineering and Applied Sciences, [∥]Kavli Nanoscience Institute, and [⊥]Beckman Institute, California Institute of Technology, Pasadena, California 91125, United States

Supporting Information

ABSTRACT: Au was photoelectrochemically deposited onto cylindrical or tapered p-Si microwires on Si substrates to profile the photoinduced charge-carrier generation in individual wires in a photoactive semiconductor wire array. Similar experiments were repeated for otherwise identical Si microwires doped to be n-type. The metal plating profile was conformal for n-type wires, but for p-type wires was a function of distance from the substrate and was dependent on the illumination wavelength. Spatially resolved charge-carrier generation profiles were computed using full-wave electromagnetic simulations, and the localization of the deposition at the p-type wire surfaces observed experimentally correlated well with the regions of enhanced calculated carrier generation in the volumes of the microwires. This technique could potentially be extended to determine the spatially resolved carrier generation profiles in a variety of mesostructured, photoactive semiconductors.

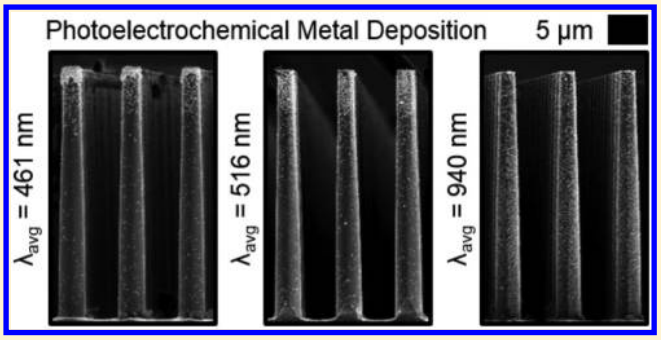

KEYWORDS: *Semiconductor, silicon, microwires, electrodeposition, photoelectrochemistry, carrier generation*

Semiconductor mesostructures have been studied extensively due to their unique band gap energies, absorption and reflectance properties, charge-transport pathways, and increased surface area, relative to their planar counterparts.[1−4] The ability to tailor such properties has made mesostructures attractive architectures for applications in areas including photonics,[5−7] photovoltaics,[8−11] electronics,[12,13] catalysis,[14−16] and sensing.[17,18] Mesostructured semiconducting wire arrays composed of elemental, binary compounds (e.g., group III−V, II−VI, IV−VI) and ternary compounds have been synthesized.[4,19−26] The macroscopic optoelectronic and electrochemical properties of such wire arrays have been experimentally characterized,[27−31] but nanoscale analyses that aim to provide a microscopic understanding of these properties have been mostly limited to theoretical and computational methodologies.[32−35]

The optical excitation of photoactive semiconductor substrates immersed in a metal−ion solution can provide the driving force for deposition of a metal.[36] Photoelectrochemical metal deposition has been used to generate arbitrarily patterned metallic deposits on semiconductor surfaces by use of a photomask or by use of scanning laser illumination.[37−41] The localized illumination results in the spatially confined generation of mobile charge-carriers that are transported toward the solid/solution interface and, subsequently, drive localized electrochemical deposition. Herein, we demonstrate the use of such a photoelectrochemical deposition process to physically record the localization of carrier generation in three-dimensional semiconductor mesostructures under conformal illumination. Unlike planar materials, such structures display significant, inherent spatially anisotropic and complex, light absorption in three dimensions.[34,35] Si microwire arrays can be grown with a high degree of fidelity and control; provide superior optical absorbance on a per unit mass basis than planar Si; and have shown potential for use in photovoltaic, fuel-forming photoelectrochemical, and sensing applications.[42−46] In this work, Au was photoelectrodeposited onto arrays of cylindrical or tapered Si microwires, using a series of narrowband light sources providing excitation at a variety of wavelengths. The localization of the Au deposition was examined by scanning electron microscopy (SEM). Computer modeling of carrier generation in the same structures was performed to correlate the localization of the deposition with the expected spatial distribution of the carrier generation in the material.

Si microwire arrays were fabricated from planar Si wafers via an inductively coupled plasma reactive-ion etching process (ICP-RIE), as described in the Supporting Information. The p-Si microwire arrays had a ∼3 μm wire diameter, 30 μm wire height, and 7 μm wire pitch in a square lattice. Au was photoelectrochemically deposited onto freshly etched wires from an aqueous solution of 0.010 M $HAuCl_4$ and 0.100 M

Received: May 2, 2016
Revised: June 7, 2016
Published: June 20, 2016

DOI: 10.1021/acs.nanolett.6b01782
Nano Lett. 2016, 16, 5015−5021

KCl. Deposition was effected by biasing the microwire array potentiostatically at −1.25 V vs Ag/AgCl (3 M) until a cathodic charge density of 0.10 C cm^{-2} had been passed. The illumination was provided from a selected narrowband light-emitting diode (LED). At this applied potential, the deposition current density under illumination was ∼5 times the deposition current density in the absence of illumination (Figure S1).

Figure 1a presents a cross-sectional SEM of a Si microwire array onto which Au was photoelectrodeposited using a LED

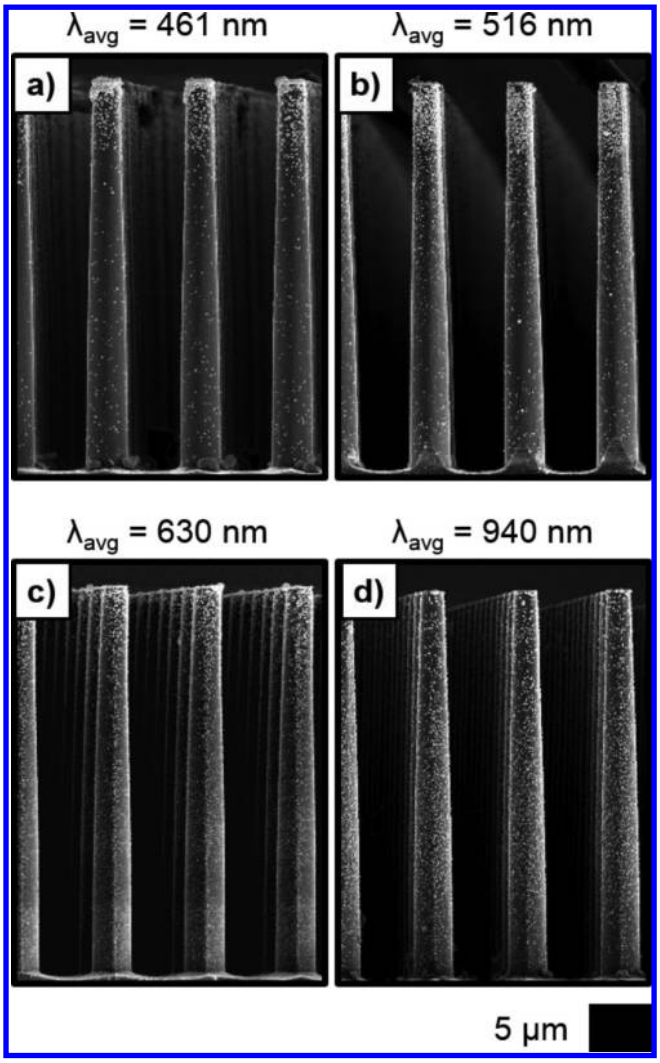

Figure 1. (a−d) Representative SEMs of p-Si microwire arrays with a ∼3 μm wire diameter, 7 μm wire pitch, and 30 μm wire height in a square lattice, upon which Au was photoelectrodeposited from a $HAuCl_4$ solution with a charge density of 0.10 C cm^{-2} using narrowband LED illumination having λ_{avg} as indicated.

with an intensity-weighted average wavelength, λ_{avg}, of 461 nm. The Au plating was radially symmetric, but enhanced deposition was observed at the tips of the wires, with the deposition diminishing rapidly along the axial dimension. Figures 1b−d present analogous SEMs for depositions using LEDs having λ_{avg} values of 516, 630, and 940 nm, respectively. Increasing λ_{avg} decreased the axial deposition gradient, with conformal deposition being approached for λ_{avg} = 940 nm. In contrast, deposition of Au proceeded conformally onto n-type Si microwire arrays that had nominally equivalent morphologies to the p-type Si microwire arrays. Figure 2a−d presents

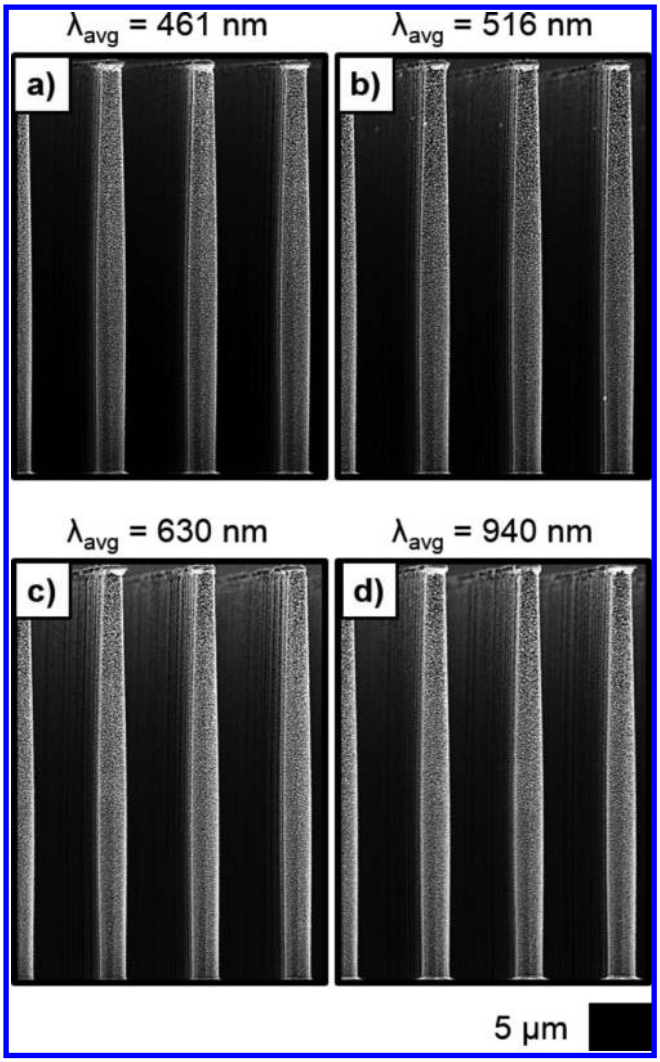

Figure 2. (a−d) Representative SEMs of n-Si microwire arrays with a ∼3 μm wire diameter, 7 μm wire pitch, and 30 μm wire height in a square lattice, upon which Au was photoelectrodeposited from a $HAuCl_4$ solution with a charge density of 0.10 C cm^{-2} using narrowband LED illumination having λ_{avg} as indicated.

representative cross-sectional SEMs analogous to those presented for the p-type arrays in Figure 1a−d. Such behavior supports a notion that the anisotropic deposition observed on the p-type Si microwire arrays is directed by light absorption and photocarrier generation and transport, as opposed to solution-based transport limitations in the void volume of the Si microwire array. Electrodeposition at a p-type semiconductor interface at a negative potential at room temperature without illumination is ineffective due to a scarcity of mobile electrons (minority carriers) in the material under such conditions. However, light absorption in p-type materials results in the generation of mobile electrons, which can approach the interface and drive electrochemical reduction reactions. Anisotropic light absorption may therefore result in anisotropic deposition at the interface of a p-type material. In contrast, at an n-type semiconductor interface, cathodic deposition does not require illumination to proceed at significant rates due to the presence of mobile electrons (majority carriers) in the material.

Computer modeling of photocarrier generation in illuminated Si microwire arrays was performed to assess the

DOI: 10.1021/acs.nanolett.6b01782
Nano Lett. 2016, 16, 5015−5021

correlation between the localization of the carrier generation and the location of metal deposition on p-type arrays. Three-dimensional, full-wave electromagnetic, finite-difference time-domain (FDTD) simulations were performed to compute the spatially resolved photocarrier generation rates in wires in arrays under plane-wave illumination. The rates are effectively independent of doping because the typically used dopant concentrations are sufficiently small that they do not affect the optical properties of the Si. Simulations were performed considering wire arrays that had similar dimensions to those utilized for photoelectrodeposition, under the same illumination profiles as those provided by the LEDs.

Figure 3a depicts a two-dimensional representation (side-view) of the simulated photocarrier generation rates in a

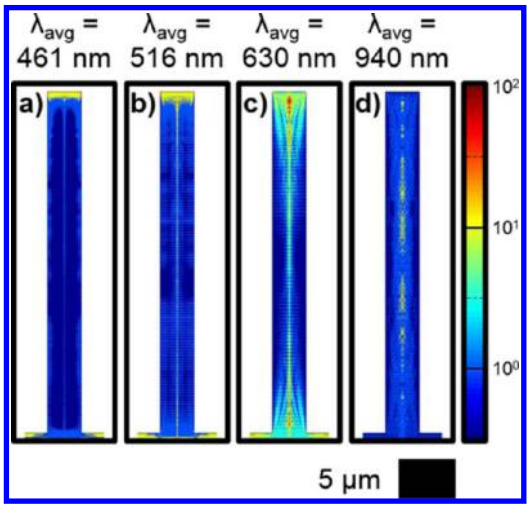

Figure 3. (a–d) Simulated relative photocarrier generation rates in Si microwires with a 3 μm wire diameter and 30 μm wire height in a square lattice with a 7 μm wire pitch under narrowband illumination with spectral profiles having λ_{avg} as indicated.

microwire under simulated illumination with λ_{avg} = 461 nm. The simulated generation in a well-defined, narrow region near the tip of the wire was at least an order of magnitude higher than in any other volume of the wire, including that directly below in the axial dimension. The photoelectrodeposition of Au at this wavelength (Figure 1a) mirrored this localization in that the majority of the Au plated near the tip of the wire. Figure 3b–d display representations of the photocarrier generation rates analogous to that presented in Figure 3a but with values of λ_{avg} of 516, 630, and 940 nm, respectively. At these longer wavelengths, the carrier generation profiles displayed waveguide characteristics that are more readily apparent than for λ_{avg} = 461 nm, due to the high Si absorption coefficient at this wavelength. Waveguide behavior was observed despite microscale wire dimensions, consistent with previous reports on semiconductor nanowire absorption.[1,47] For λ_{avg} = 516 nm, as with λ_{avg} = 461 nm, generation near the tip of the wire was generally at least an order of magnitude higher than at other axial locations in the microwire. For λ_{avg} = 516 nm, the region of high generation near the tip was thicker, and generation throughout the rest of the volume was mostly equivalent or higher than the profile calculated for λ_{avg} = 461 nm. The localization of carrier generation for λ_{avg} = 516 nm was also similar to that observed experimentally for Au photoelectrodeposition, as shown in Figure 1b, where the plating was concentrated axially in a region near the tip of the wire, but with diminished axial anisotropy relative to the deposition under λ_{avg} = 461 nm illumination. For λ_{avg} = 630 nm, the carrier generation profile was significantly more isotropic than for the shorter wavelength cases. However, the total generation in the ~5 μm axial sections at the top and bottom of the wire was greater than that in the center of the wire. This calculated generation profile matched the photoelectrodeposition profile observed experimentally (Figure 1c), wherein significant Au plating was observed along the entire length of the wires, but with somewhat greater density at the tops and bottoms. For λ_{avg} = 940 nm, the calculated carrier generation was more uniform in the axial dimension than for λ_{avg} = 630 nm. The total generation was somewhat lower in the top and bottom ~5 μm of the wire relative to the generation in the center. The Au plating (Figure 1d) mirrored this observation, with generally conformal deposition that was nevertheless lower at the very top and bottom relative to the center. Thus, the localization of photocarrier generation consistently agreed with the localization of the photoelectrodeposited Au, indicating that the cathodic metal plating is directed by carrier generation in the p-type material under the conditions utilized in this work. Such a phenomenon indicates that the micrographs of the metal deposition provide a spatially resolved image of the relative photocarrier generation rates in structured semiconductors, provided that carrier transport occurs over sufficiently short distances to maintain the integrity of the linkage between the locations of volumetric carrier generation and the minority carrier flux that produces surface-based metal deposition.

To examine the capability of the photoelectrodeposition process to profile photocarrier generation in arbitrary mesostructured semiconductor arrays, several p-Si tapered microwire arrays were evaluated. As with the cylindrical microwires investigated herein, each tapered wire array consisted of structures that were ~30 μm in height on a 7 μm pitch in a square lattice. As with the cylindrical wires, the tapered wires had a diameter of ~3 μm at the tips of the wires. The tapered wires had, however, a ratio of their base diameter to tip diameter, ρ, of 1.4, 1.6, or 2.3 (ρ = 1 for cylindrical wires). For wires with ρ = 1.4 and 1.6, the wire diameter tapered linearly from tip to base, whereas for wires with ρ = 2.3 the diameter tapered nonlinearly, producing a bottle-like shape. Figure 4a–c depicts two-dimensional representations (side-view) of the simulated photocarrier generation rates in tapered microwires with ρ = 1.4, 1.6, and 2.3, respectively, under simulated illumination with λ_{avg} = 461 nm. In each case, the simulations indicated the presence of a narrow, well-defined region at the very tip of the wires where the generation was approximately an order of magnitude higher than in any other region in the microwire volume, as observed for the cylindrical wire at this wavelength (Figure 3a). For ρ = 1.6, a radially thin region of elevated generation, extending 10 μm down from the tip in the axial dimension, was observed in the radial center of the wire. This behavior was, however, not observed for other values of ρ at this wavelength. For ρ = 2.3, the generation at the wire sidewalls was enhanced compared to the other structures, in a manner consistent with increased collection of normal incidence photons due to the significant taper.

Figure 4d–f, g–i, and j–l present data analogous to that in Figure 4a–c but using simulated illumination with λ_{avg} values of 516, 630, and 940 nm, respectively. As with the case of the cylindrical wires, at these wavelengths, enhanced coupling to the waveguide mode was observed in the generation profiles. For λ_{avg} = 516 nm, and for wires with every value of ρ, the

DOI: 10.1021/acs.nanolett.6b01782
Nano Lett. 2016, 16, 5015–5021

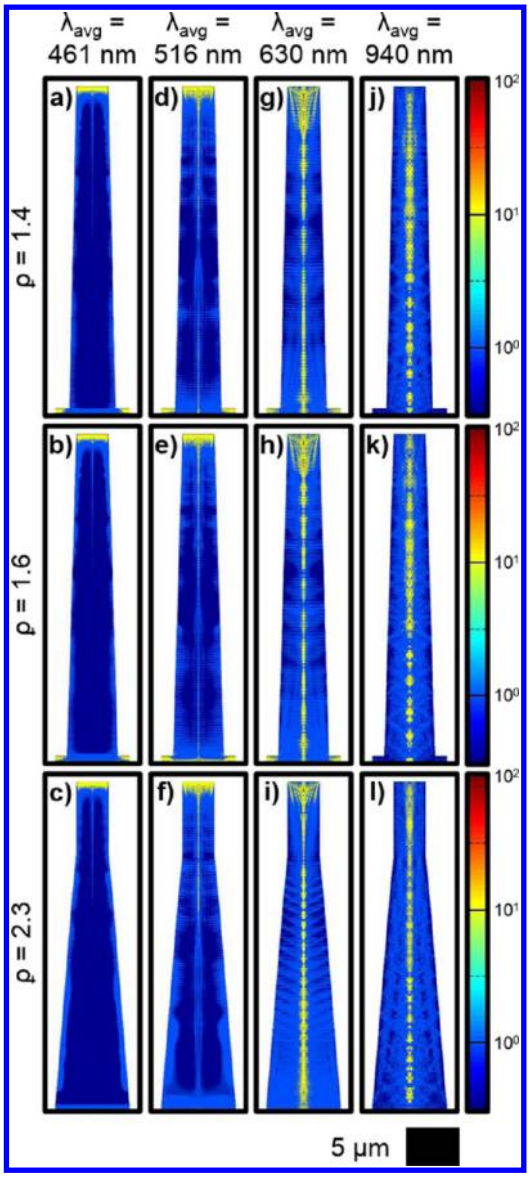

Figure 4. (a–l) Simulated relative photocarrier generation rates in tapered Si microwires with a 3 μm wire top diameter and 30 μm wire height in a square lattice with a 7 μm wire pitch under narrowband illumination with spectral profiles having λ_{avg} as indicated. The ratio of the wire diameter at the base to that at the top (ρ) is indicated.

simulations each exhibited an axially well-defined, radially thick, region of high generation near the top of the wire, with a radially thin region of similarly high generation extending for several microns directly below through the radial center of the wire. Such results were consistent with the cylindrical case (Figure 3b). However, for ρ = 1.4, the region of radially thin high generation extending below the tip was more pronounced and extended >5 μm down the axial dimension. For ρ = 1.6, this same region extended approximately midway down the axial dimension of the wire, and a second, similarly shaped, high generation region was observed in the bottom quarter of the wire. For ρ = 2.3, the region of high generation extending below the tip was axially shorter than observed for the other shapes, but an isolated, radially thin region of high generation, <5 μm long in the axial dimension, was observed ~10 μm from the top of the wire. Enhanced generation at the sidewalls was also observed for ρ = 2.3 relative to the other shapes, consistent with the observations for λ_{avg} = 461 nm. For λ_{avg} = 630 nm, the simulated generation in the tapered wires was generally described by a region of radially thick high generation near the tips of the wires, with similarly high generation in a radially thin region at the wire center throughout the entire axial length. The region of radially thick high generation near the tips was longer in the axial dimension for all values of ρ with λ_{avg} = 630 nm than with λ_{avg} = 461 or 516 nm. However, the axial length of this region decreased as ρ increased. For ρ = 1.4, less generation in the second quarter from the top of the wire and additional generation in the bottom quarter were observed relative to the wires with greater ρ values. For λ_{avg} = 940 nm, a significant concentration of generation in the wire tip relative to the rest of the microwire volume was not observed for any value of ρ. Rather, the carrier generation was generally consistent in the axial dimension, with highest generation concentrated in the center of the wire volume. However, as ρ increased, the generation did appear to decrease somewhat in the bottom half of the wire.

Figure 5 presents experimental data complementary to the modeling data shown Figure 4 and is arranged in an analogous fashion. Specifically, Figure 5a–l presents cross-sectional SEMs of tapered p-Si microwire arrays with values of ρ = 1.4, 1.6, and 2.3, wherein Au was photoelectrodeposited with LEDs having λ_{avg} values of 461, 516, 630, and 940 nm, respectively, in the same manner as for the cylindrical wires (Figure 1). At every value of ρ, photoelectrodeposition with λ_{avg} = 461 nm illumination resulted in very dense Au plating at the very tip of the wires, consistent with the well-defined, narrow high-generation region indicated by the simulations in this volume of the wires (Figure 4a–c) and with the behavior observed for the cylindrical case (Figure 1a). For ρ = 1.6, photoelectrodeposition was also observed below the tip in the top half of the wires, consistent with elevated generation observed via simulation in the center and near the sidewalls in this volume of the wire (Figure 4b). Similarly, for ρ = 2.3, sparse deposition was observed over the full axial dimension below the tip, consistent with the simulated prediction of elevated sidewall generation (Figure 4c). Photoelectrochemical Au plating with λ_{avg} = 516 nm illumination on wires with ρ = 1.4 resulted in a gradient of deposition in the top half of the wire, wherein dense plating near the tip transitioned to sparse near the axial midpoint. For ρ = 1.6, significant deposition was observed from the top of the wire down to the axial midpoint and also in the axial bottom quarter. This result is consistent with the simulations (Figure 4d,e), which indicated significantly enhanced generation rates in the same axial segments for which Au plating was observed. For ρ = 2.3, heavy plating was observed near the top of the wire, with substantial, but less dense, deposition in axial top half and sparse deposition in the bottom half. The relatively higher deposition in the top half of this structure is consistent with the prediction of generation concentration in this volume (Figure 4f). Utilization of λ_{avg} = 630 nm illumination for deposition on wires with ρ = 1.4 resulted in significant deposition over the axial top quarter and bottom half of the wires and sparser deposition over the second quarter. Deposition with λ_{avg} = 630 nm illumination on wires with ρ = 1.6 and ρ = 2.3 resulted in a gradient of Au plating, with significant deposition at tops of the wires and sparse deposition near the bottoms. These results are consistent with the concentration of generation along the axial dimension of the wires, as predicted by the simulations (Figure 4g–i). Deposition with λ_{avg} = 940 nm illumination on wires with ρ = 1.4 resulted in relatively conformal plating. This

DOI: 10.1021/acs.nanolett.6b01782
Nano Lett. 2016, 16, 5015–5021

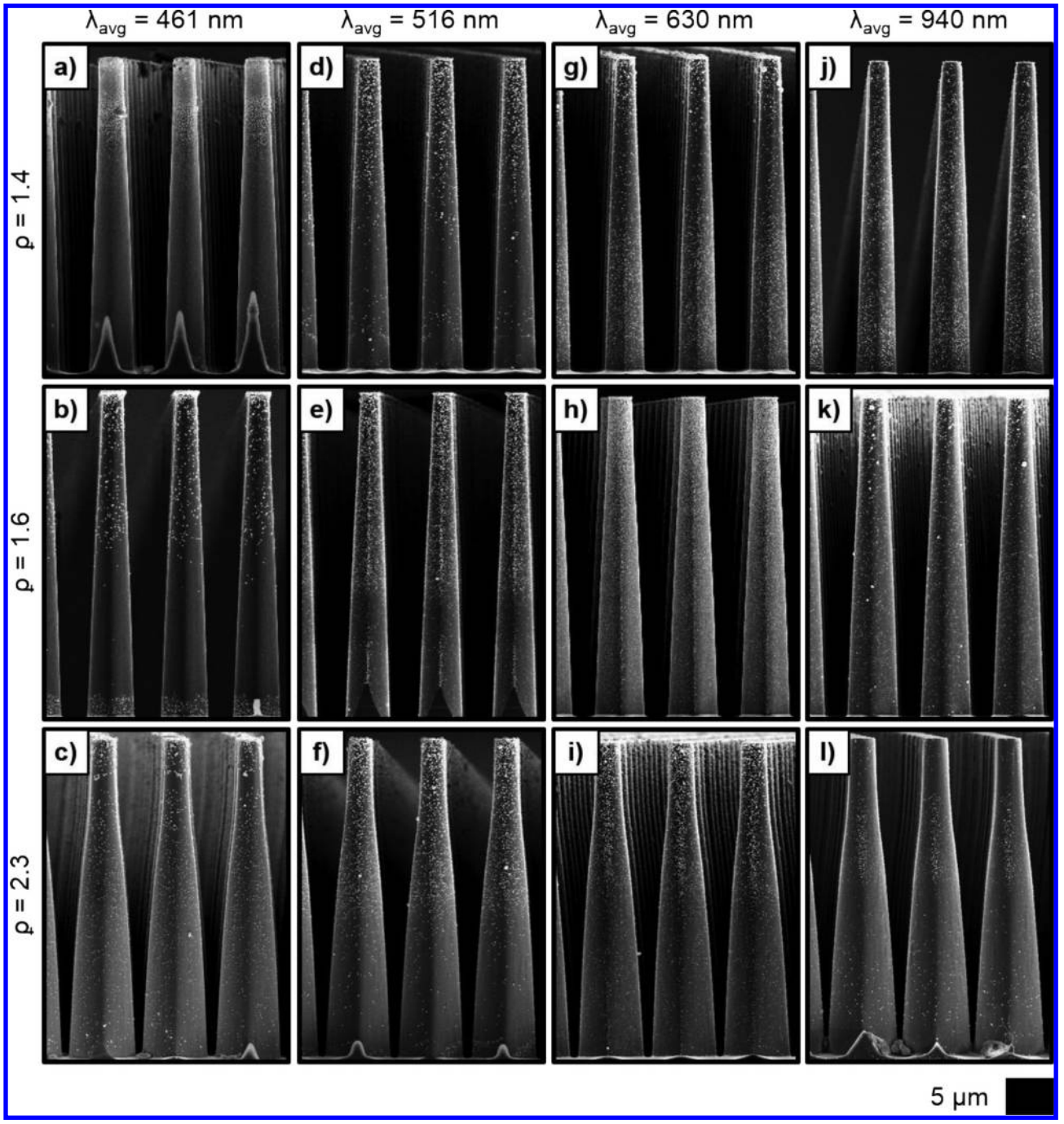

Figure 5. (a–l) Representative SEMs of tapered p-Si microwire arrays with a ~3 μm wire top diameter, 7 μm wire pitch, and 30 μm wire height in a square lattice, upon which Au was photoelectrodeposited from a $HAuCl_4$ solution with a charge density of 0.10 C cm^{-2} using narrowband LED illumination having λ_{avg} as indicated. The ratio of the wire diameter at the base to that at the top (ρ) is indicated.

conformality matched the lack of axial generation concentration indicated by the modeling (Figure 4j). Results for deposition with λ_{avg} = 940 nm illumination on wires with ρ = 1.6 and 2.3 were similar, but with sparser deposition in the axial bottom halves of the wires. The simulations predict a similar amount of total generation in these structures as for those with ρ = 1.4, but because the spatial volume is larger, the generation concentration is lower, consistent with the experimental observations.

The collective data suggest that the spatially varying relative charge-carrier generation rates in a p-type semiconductor mesostructure under illumination can be physically recorded via cathodic photoelectrodeposition of a metal. For each p-Si microwire array and illumination spectrum investigated, the localization of Au deposited photoelectrochemically on the surface directly correlated with the relative concentration of carrier generation in the adjacent volume of the structure, as determined by computer simulation. In this work, computational assessment of the spatial dependence of charge-carrier generation was in part enabled by the high degree of uniformity and symmetry in the wire arrays. Each wire was considered as an identical element in a semi-infinite square lattice, and periodic boundary conditions were utilized to simulate a macroscopic array by considering only a microscale volume.

DOI: 10.1021/acs.nanolett.6b01782
Nano Lett. 2016, 16, 5015–5021

Analysis of mesostructures without significant uniformity and order thus could be computationally intractable, but still carried out rapidly via the photoelectrochemical profiling technique described herein. This method may be of particular interest for interrogation of materials generated by low temperature, wet-chemical, and maskless techniques.[48−53] In this work, Si was utilized for demonstration, but since the imaging relies only on the light absorption and charge separation abilities intrinsic to semiconductors, the method should be readily generalizable to a wide class of materials. Similarly, Au was utilized as the marker material, but any metal that can be electrochemically deposited in a potential window compatible with the semiconductor may also be utilized. Additionally, while in this work cathodic deposition was used to record generation on a p-type material, n-type materials may be similarly treated using oxidative deposition to apply the marker or even possibly by anodization of the material itself.[54,55] Anodic photoelectrochemical etching of semiconductor surfaces using illumination with spatially varying intensity has been used to generate microlenses, diffraction gratings, and transformation optics.[56−58] Moreover, the potential to direct spatially localized deposition on an array of semiconductor materials and morphologies suggests that photoelectrodeposition may be used as a template-free technique to selectively decorate semiconductor surfaces. This strategy could utilize conformal illumination without a photomask and thus potentially generate features with sizes unconstrained by the optical diffraction limit. The deposition anisotropy could then be controlled by varying the excitation spectra to tune the spatial concentration of carrier generation in the structures.[59] Such a methodology may be utilized to place reflector materials for photovoltaic applications, catalysts for photoelectrochemical fuel generation systems, and conductive contacts for microelectronics.[60−65]

In summary, photoelectrochemical deposition of Au onto cylindrical p-Si microwire arrays resulted in spatially anisotropic metal plating at the microwire surface, wherein the localization of the plating was a function of the illumination wavelength. The same deposition process was repeated with n-Si wire arrays, and conformal deposition was observed regardless of wavelength. The spatial distribution of the photoinduced charge-carrier generation rates in the wires, as derived from computer simulations using a FDTD method, correlated well with the localization of the metal deposition observed experimentally. Analogous simulations of the spatially resolved photocarrier generation rates in a series of related p-Si microwire arrays with tapered (noncylindrical) wires was also performed. Photoelectrodeposition was then performed on wires arrays with equivalent morphologies to those simulated, and the metal plating at the wire surfaces was observed to be a function of carrier generation concentration in the adjacent wire volume. The photoelectrodeposition of metals on semiconductor mesostructures thus appears to be of use for profiling charge-carrier generation in such structures. Additionally, the technique appears to be of potential use for maskless, directed deposition of materials with subwavelength features.

■ ASSOCIATED CONTENT

Supporting Information

The Supporting Information is available free of charge on the ACS Publications website at DOI: 10.1021/acs.nanolett.6b01782.

Additional details regarding experimental and computer modeling methods and voltammetry data (PDF)

■ AUTHOR INFORMATION

Corresponding Author

*E-mail: nslewis@caltech.edu.

Author Contributions

M.D. and A.I.C. contributed equally to this work.

Notes

The authors declare no competing financial interest.

■ ACKNOWLEDGMENTS

This work was supported by the "Light−Material Interactions in Energy Conversion" Energy Frontier Research Center funded by the U.S. Department of Energy, Office of Science, Office of Basic Energy Sciences under Award Number DE-SC0001293. The computational methods in this work used resources of the National Energy Research Scientific Computing Center, a DOE Office of Science User Facility supported by the Office of Science of the U.S. Department of Energy under Contract No. DE-AC02-05CH11231. This work was also supported in part by the National Science Foundation under Grant No. CHE-1214152 (support for N.S.L.). M.D. acknowledges a Postdoctoral Fellowship from the National Sciences and Engineering Research Council of Canada. A.I.C. acknowledges a Graduate Research Fellowship from the National Science Foundation. The authors gratefully acknowledge R. Jones and Dr. K. Walczak for assistance with photoelectrochemical cell fabrication.

■ REFERENCES

(1) Cao, L.; White, J. S.; Park, J. S.; Schuller, J. A.; Clemens, B. M.; Brongersma, M. L. *Nat. Mater.* **2009**, *8*, 643−647.
(2) Liu, S.; Tang, Z. R.; Sun, Y.; Colmenares, J. C.; Xu, Y. J. *Chem. Soc. Rev.* **2015**, *44*, 5053−5075.
(3) Dasog, M.; Kehrle, J.; Rieger, B.; Veinot, J. G. *Angew. Chem., Int. Ed.* **2016**, *55*, 2322−2339.
(4) Wang, F.; Dong, A.; Buhro, W. E. *Chem. Rev.* **2016**, DOI: 10.1021/acs.chemrev.5b00701.
(5) Shields, A. J. *Nat. Photonics* **2007**, *1*, 215−223.
(6) Hoffman, A. J.; Alekseyev, L.; Howard, S. S.; Franz, K. J.; Wasserman, D.; Podolskiy, V. A.; Narimanov, E. E.; Sivco, D. L.; Gmachl, C. *Nat. Mater.* **2007**, *6*, 946−950.
(7) Yan, R.; Gargas, D.; Yang, P. *Nat. Photonics* **2009**, *3*, 569−576.
(8) Nozik, A. J.; Beard, M. C.; Luther, J. M.; Law, M.; Ellingson, R. J.; Johnson, J. C. *Chem. Rev.* **2010**, *110*, 6873−6890.
(9) Nozik, A. J. *Nano Lett.* **2010**, *10*, 2735−2741.
(10) Boix, P. P.; Lee, Y. H.; Fabregat-Santiago, F.; Hyuk, S.; Imanishi, Y.; Mora-Sero, I.; Bisquert, J.; Seok, S. I. *ACS Nano* **2012**, *6*, 873−880.
(11) Carey, G. H.; Abdelhady, A. L.; Ning, Z.; Thon, S. M.; Bakr, O. M.; Sargent, E. H. *Chem. Rev.* **2015**, *115*, 12732−12763.
(12) Kim, F. S.; Ren, G.; Jenekhe, S. A. *Chem. Mater.* **2011**, *23*, 682−732.
(13) Price, P. J. *IEEE Trans. Electron Devices* **1981**, *28*, 911−914.
(14) Kamat, P. V. *J. Phys. Chem. C* **2007**, *111*, 2834−2860.
(15) Navarro Yerga, R. M.; Alvarez Galvan, M. C.; del Valle, F.; Villoria de la Mano, J. A.; Fierro, J. L. *ChemSusChem* **2009**, *2*, 471−485.
(16) Walter, M. G.; Warren, E. L.; McKone, J. R.; Boettcher, S. W.; Mi, Q.; Santori, E. A.; Lewis, N. S. *Chem. Rev.* **2010**, *110*, 6446−6473.
(17) Murphy, C. J. *Anal. Chem.* **2002**, *74*, 520−526.
(18) Kolmakov, A.; Moskovits, M. *Annu. Rev. Mater. Res.* **2004**, *34*, 151−180.
(19) Kayes, B. M.; Filler, M. A.; Putnam, M. C.; Kelzenberg, M. D.; Lewis, N. S.; Atwater, H. A. *Appl. Phys. Lett.* **2007**, *91*, 103110.

DOI: 10.1021/acs.nanolett.6b01782
Nano Lett. 2016, 16, 5015−5021

(20) Wu, Y.; Yan, H.; Yang, P. *Top. Catal.* **2002**, *19*, 197−202.
(21) Duan, X.; Wang, J.; Lieber, C. M. *Appl. Phys. Lett.* **2000**, *76*, 1116−1118.
(22) Yang, Y.; Kung, S. C.; Taggart, D. K.; Xiang, C.; Yang, F.; Brown, M. A.; Güell, A. G.; Kruse, T. J.; Hemminger, J. C.; Penner, R. M. *Nano Lett.* **2008**, *8*, 2447−2451.
(23) Li, L.; Yang, Y.; Huang, X.; Li, G.; Zhang, L. *J. Phys. Chem. B* **2005**, *109*, 12394−12398.
(24) Wu, Y.; Yan, H.; Huang, M.; Messer, B.; Song, J. H.; Yang, P. *Chem. - Eur. J.* **2002**, *8*, 1260−1268.
(25) Routkevitch, D.; Tager, A. A.; Haruyama, J.; Almalwai, D.; Moskovits, M.; Xu, J. M. *IEEE Trans. Electron Devices* **1996**, *43*, 1646−1658.
(26) Collins, S. M.; Hankett, J. M.; Carim, A. I.; Maldonado, S. *J. Mater. Chem.* **2012**, *22*, 6613−6622.
(27) Vo, T.; Williamson, A. J.; Galli, G. *Phys. Rev. B: Condens. Matter Mater. Phys.* **2006**, *74*, 045116.
(28) Park, W. I.; Zheng, G.; Jiang, X.; Tian, B.; Lieber, C. M. *Nano Lett.* **2008**, *8*, 3004−3009.
(29) Yao, M.; Huang, N.; Cong, S.; Chi, C. Y.; Seyedi, M. A.; Lin, Y. T.; Cao, Y.; Povinelli, M. L.; Dapkus, P. D.; Zhou, C. *Nano Lett.* **2014**, *14*, 3293−3303.
(30) Xiang, C.; Meng, A. C.; Lewis, N. S. *Proc. Natl. Acad. Sci. U. S. A.* **2012**, *109*, 15622−15627.
(31) Kempa, T. J.; Day, R. W.; Kim, S.-K.; Park, H.-G.; Lieber, C. M. *Energy Environ. Sci.* **2013**, *6*, 719.
(32) Fountaine, K. T.; Atwater, H. A. *Opt. Express* **2014**, *22*, A1453−A1461.
(33) Alaeian, H.; Atre, A. C.; Dionne, J. A. *J. Opt.* **2012**, *14*, 024006.
(34) Fountaine, K. T.; Whitney, W. S.; Atwater, H. A. *J. Appl. Phys.* **2014**, *116*, 153106.
(35) Fountaine, K. T.; Kendall, C. G.; Atwater, H. A. *Opt. Express* **2014**, *22*, A930−A940.
(36) Hotsenpiller, P. A. M.; Bolt, J. D.; Farneth, W. E.; Lowekamp, J. B.; Rohrer, G. S. *J. Phys. Chem. B* **1998**, *102*, 3216−3226.
(37) Attard, A. E.; Brown, D. E. *Appl. Opt.* **1968**, *7*, 511−516.
(38) Inoue, T.; Fujishima, A.; Honda, K. *J. Electrochem. Soc.* **1980**, *127*, 1582−1588.
(39) Morishita, S. *Chem. Lett.* **1992**, *21*, 1979−1982.
(40) Yoshihara, S.; Shinozaki, K.; Shirakashi, T.; Hashimoto, K.; Tryk, D. A.; Fujishima, A. *Electrochim. Acta* **1999**, *44*, 2711−2719.
(41) Micheels, R. H.; Darrow, A. D.; Rauh, R. D. *Appl. Phys. Lett.* **1981**, *39*, 418−420.
(42) Kelzenberg, M. D.; Boettcher, S. W.; Petykiewicz, J. A.; Turner-Evans, D. B.; Putnam, M. C.; Warren, E. L.; Spurgeon, J. M.; Briggs, R. M.; Lewis, N. S.; Atwater, H. A. *Nat. Mater.* **2010**, *9*, 239−244.
(43) Gharghi, M.; Fathi, E.; Kante, B.; Sivoththaman, S.; Zhang, X. *Nano Lett.* **2012**, *12*, 6278−6282.
(44) Warren, E. L.; Atwater, H. A.; Lewis, N. S. *J. Phys. Chem. C* **2014**, *118*, 747−759.
(45) Boettcher, S. W.; Spurgeon, J. M.; Putnam, M. C.; Warren, E. L.; Turner-Evans, D. B.; Kelzenberg, M. D.; Maiolo, J. R.; Atwater, H. A.; Lewis, N. S. *Science* **2010**, *327*, 185−187.
(46) Park, I.; Li, Z.; Pisano, A. P.; Williams, R. S. *Nanotechnology* **2010**, *21*, 015501.
(47) Abujetas, D. R.; Paniagua-Domínguez, R.; Sánchez-Gil, J. A. *ACS Photonics* **2015**, *2*, 921−929.
(48) Choi, K.-S. *Dalton Trans.* **2008**, 5432−5438.
(49) McShane, C. M.; Choi, K.-S. *J. Am. Chem. Soc.* **2009**, *131*, 2561−2569.
(50) Carim, A. I.; Collins, S. M.; Foley, J. M.; Maldonado, S. *J. Am. Chem. Soc.* **2011**, *133*, 13292−13295.
(51) Wang, F.; Wayman, V. L.; Loomis, R. A.; Buhro, W. E. *ACS Nano* **2011**, *5*, 5188−5194.
(52) Carim, A. I.; Batara, N. A.; Premkumar, A.; Atwater, H. A.; Lewis, N. S. *ACS Nano* **2016**, *10*, 102−111.
(53) Penner, R. M. *J. Phys. Chem. C* **2014**, *118*, 17179−17192.
(54) Kohl, P. A. *IBM J. Res. Dev.* **1998**, *42*, 629−637.
(55) Zhao, Y.; Vargas-Barbosa, N. M.; Hernandez-Pagan, E. A.; Mallouk, T. E. *Small* **2011**, *7*, 2087−2093.
(56) Ostermayer, F. W.; Kohl, P. A.; Burton, R. H. *Appl. Phys. Lett.* **1983**, *43*, 642−644.
(57) Lum, R. M.; Glass, A. M.; Ostermayer, F. W.; Kohl, P. A.; Ballman, A. A.; Logan, R. A. *J. Appl. Phys.* **1985**, *57*, 39−44.
(58) Barth, D. S.; Gladden, C.; Salandrino, A.; O'Brien, K.; Ye, Z.; Mrejen, M.; Wang, Y.; Zhang, X. *Adv. Mater.* **2015**, *27*, 6131−6136.
(59) Carim, A. I.; Batara, N. A.; Premkumar, A.; Atwater, H. A.; Lewis, N. S. *Nano Lett.* **2015**, *15*, 7071−7076.
(60) Hu, L.; Chen, G. *Nano Lett.* **2007**, *7*, 3249−3252.
(61) Kang, D.; Kim, T. W.; Kubota, S. R.; Cardiel, A. C.; Cha, H. G.; Choi, K. S. *Chem. Rev.* **2015**, *115*, 12839−12887.
(62) Heller, A.; Vadimsky, R. G. *Phys. Rev. Lett.* **1981**, *46*, 1153−1156.
(63) Aharon-Shalom, E.; Heller, A. *J. Electrochem. Soc.* **1982**, *129*, 2865−2866.
(64) Heller, A.; Aspnes, D. E.; Porter, J. D.; Sheng, T. T.; Vadimsky, R. G. *J. Phys. Chem.* **1985**, *89*, 4444−4452.
(65) Wu, W. W.; Lu, K. C.; Wang, C. W.; Hsieh, H. Y.; Chen, S. Y.; Chou, Y. C.; Yu, S. Y.; Chen, L. J.; Tu, K. N. *Nano Lett.* **2010**, *10*, 3984−3989.

DOI: 10.1021/acs.nanolett.6b01782
Nano Lett. 2016, 16, 5015−5021